Journal of Statistical Physics, Vol. 15, No. 6, 1976

Statistical Dynamics of the Lorenz Model

M. Lücke[1,2]

Received April 27, 1976

The dynamics of the Lorenz model in the "turbulent" regime ($r > r_T$) is investigated by applying methods for treating many-body systems. Symmetry properties are used to derive relations between correlation functions. The basic ones are evaluated numerically and discussed for several values of the parameter r. A theory for the spectra of the two independent relaxation functions is presented using a dispersion relation representation in terms of relaxation kernels and characteristic frequencies. Their role in the dynamics of the system is discussed and it is shown that their numerical values increase in proportion to $\sqrt{r}$. The approximation of the relaxation kernels that represent nonlinear coupling between the variables by a relaxation time expression and a simple mode coupling approximation, respectively, is shown to explain the two different fluctuation spectra. The coupling strength for the modes is determined by a Kubo relation imposing self-consistency. Comparison with the "experimental" spectra is made for three values of r.

KEY WORDS: Turbulence; Rayleigh–Bénard layer; random behavior of nonlinear differential equations; fluctuation spectra; dispersion relation representation; relaxation kernel; mode–mode coupling.

1. INTRODUCTION

The current revival of interest in turbulence[1] has quite naturally been accompanied by a more general one in systems governed by nonlinear equations exhibiting transitions to irregular behavior. As a result models originally devised in biological or meteorological contexts have not escaped the attention of physicists.

May[2] and Oster[3] showed that a wide class of simple deterministic population models used in ecology can display chaotic behavior. Varying one parameter, the solutions of the one-dimensional nonlinear difference

[1] Deutsche Forschungsgemeinschaft research fellow.

[2] Department of Physics, Harvard University, Cambridge, Massachusetts.

equations which define these models go from stable points through a sequence of bifurcations into stable cycles of increasing period and finally into a chaotic regime which may contain periodicity stripes.[3]

Reducing a model for finite-amplitude convection, Lorenz[4] discovered that a simple three-dimensional system of nonlinear differential equations showed transition to random "turbulent" behavior and discussed the form of nonperiodic orbits. In this model, also periodicity regions are imbedded[5] in the random regime. His equations describe conduction and convection reasonably well. They also describe qualitatively the onset of turbulence in Rayleigh–Bénard layers of fluids with not too small Prandtl numbers.[1,6]

One of the interesting features of the random behavior of this model is the possibility of doing statistical mechanics without introducing external noise sources.[6]

Orszag[7] investigated and demonstrated the randomness of a system of five nonlinearly coupled differential equations by numerically evaluating some correlation functions. McLaughlin[8] did numerical calculations for the Lorenz model, showing that correlations phase mix to zero.

The purpose of this paper is to elucidate the dynamics of the Lorenz model in the "turbulent" regime by applying statistical methods for treating many-body systems.

Symmetry properties of the model introduced in Section 2 are exploited in Section 3 to establish relations between correlations and reduce the number of independent relaxation functions to two. These functions are calculated numerically for several values of the parameters.

A theory to explain the dynamics of the system as displayed in the relaxation functions and the oscillatory movement in phase space is presented in Section 4. Central to this theory is a dispersion relation representation[9] of the relaxation functions generated by a Mori–Zwanzig projector formalism[10] involving relaxation kernels and characteristic frequencies. These frequencies are shown to dominate the phase space motion. They are derived and calculated as the simplest combinations of the model variables. The relaxation kernels represent nonlinear coupling of the three modes.

The result of a simple mode coupling approximation is compared with the "experimental" spectra.

2. THE MODEL

The model[4] is defined in terms of the dimensionless variables x, y, z,

$$\dot{x} = \sigma(y - x), \qquad \dot{y} = rx - y - xz, \qquad \dot{z} = -bz + xy \tag{1}$$

Applied to thermal convection in the Bénard problem,[4,6] the parameter

σ stands for the Prandtl number of the fluid, $r = R/R_c$ is the ratio of the Rayleigh number R to the critical value R_c for onset of convection. The parameter b is connected with the wave number of the convection rolls.

The variable x measures the velocity of the convective motion, z corresponds to the deviation of the vertical temperature profile from linear conduction behavior between the horizontal boundaries confining the fluid, and y measures the horizontal dependence of the above temperature deviation.

With the substitution

$$\underline{y} = y - x \tag{2}$$

(1) can be rewritten as the system of equations

$$\dot{x} = \sigma \underline{y}, \qquad \dot{\underline{y}} = (r - 1)x - (\sigma + 1)\underline{y} - xz, \qquad \dot{z} = -bz + x\underline{y} + x^2 \tag{3}$$

We prefer (3) to (1) for two technical reasons: (1) A numerical integration of (3) is easier since the average absolute size of the derivative of $\underline{y}$ is smaller than that of y. (2) $x, \underline{y}, z$ are orthogonal to each other in a sense explained in Section 3.3.

Equations (3) have three steady-state solutions: The trivial one

$$x = \underline{y} = z = 0 \tag{4}$$

represents the state of conduction which is stable for $r < 1$; the other steady-state solutions

$$x = \pm[b(r - 1)]^{1/2}; \qquad \underline{y} = 0; \qquad z = r - 1 \tag{5}$$

describe convection in left and right turning rolls and are stable for $r > 1$. For a picture showing the variables x, y, z and their relationship to observable quantities see Fig. 1 of Ref. 6.

Linear stability analysis of the convection solution (5) shows[4,6] that they become unstable for $r > r_T$,

$$r_T = \sigma \frac{\sigma + b + 3}{\sigma - b - 1} \tag{6}$$

With the values $\sigma = 10$ and $b = 8/3$ originally chosen by Salzman[11] and Lorenz[4] the threshold value r_T is 24.74. However, for $21 < r < 24.74$ there already exist finite-amplitude instabilities.[6] Beyond the "turbulence" threshold r_T, the trajectories are nonperiodic and irregular. There are, however, values of $r > r_T$ for which the system exhibits periodic motions.[5] The trajectories in the nonperiodic regimes to which we restrict ourselves

seem to belong to a "strange attractor"[12] type solution, which, being locally the product of a Cantor set and a two-dimensional surface, has measure zero in phase space.

Figure 1 shows the trajectory for $r = 30$ projected onto the x–y plane and onto the x–z plane for a time interval of 4.5. The points denote the steady-state solutions (5). The crosses indicate roughly the intersections with the x–z plane and the numbers their consecutive order. Since we are mainly interested in the statistical aspects of the trajectories as discussed in Sections 3.3 and 4.1, we refer to Refs. 4 and 6 for a detailed discussion of these trajectories.

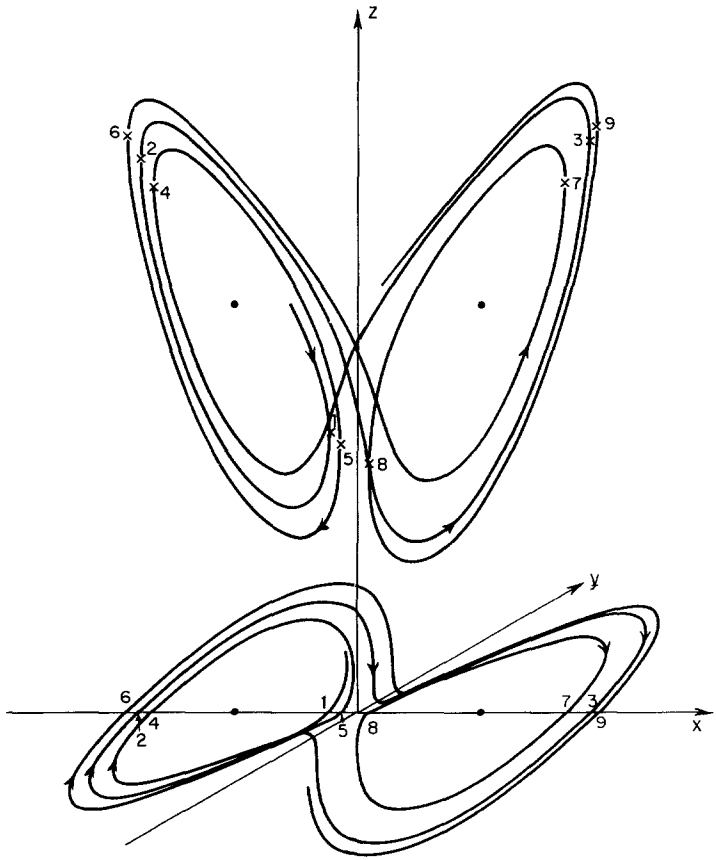

Fig. 1. Trajectory of the Lorenz model ($r = 30$, elapsed time 4.5) projected onto the x–y plane (bottom) and onto the x–z plane (top). The points are the steady-state solutions (5). Crosses indicate intersections with the x–z plane numbered according to their consecutive appearance.

3. STATISTICAL PROPERTIES OF THE SYSTEM IN THE NONPERIODIC REGIME

3.1. Averages

Let $A(t)$ be a real, well-behaved function of $x(t)$, $y(t)$, and $z(t)$ in the sense that the time average

$$\langle A \rangle_{\mathbf{X}} = \lim_{T \to \infty} \frac{1}{T} \int_0^T d\tau \, A(t + \tau) \tag{7}$$

over a trajectory specified by the initial condition $(x(t), y(t), z(t)) = \mathbf{X}$ exists. Then by definition $\langle A \rangle_{\mathbf{X}}$ is independent of t but depends in general on the trajectory. In fact, the averages we shall discuss later seem "almost" independent of the orbits. This has been confirmed numerically by calculations with randomly chosen values for $\mathbf{X}$. The restriction "almost" refers to exceptions like the steady-state points (4) and (5). Obviously they yield different averages. Since after a finite time *all* trajectories are confined to stay within a finite volume of phase space,[4] it is plausible but unproven that the averages (7) are independent of $\mathbf{X}$ with the exception of a set of points of measure zero.

Orszag's[7] numerical results for a similar five-mode system with "energy" conservation $\sum_{i=1}^{5} dx_i^2/dt = 0$ indicate that time averages over a single orbit equal space averages over the surface of constant energy for almost every orbit.

All averages reported later were calculated over trajectories specified by the initial values $z_0 = \frac{3}{4}r$, $x_0 = y_0 = \sqrt{z_0}$. The subscript $\mathbf{X}$ will thus be dropped in the following.

3.2. Symmetries and Correlations

In this section we derive the properties of correlations exploiting time translational invariance of (7) and the symmetry of the equations (3) under the parity operation $x, y \to -x, -y$. The latter symmetry requires that

$$\langle A(x, y, z) \rangle = 0 \qquad \text{if} \quad A(-x, -y, z) = -A(x, y, z) \tag{8}$$

In particular,

$$\langle x \rangle = \langle y \rangle = 0 \tag{9a}$$

$$\langle xz \rangle = \langle yz \rangle = 0 \tag{9b}$$

Time translational invariance requires that

$$\frac{d}{dt} \langle A(x, y, z) \rangle = \left\langle \frac{\partial A}{\partial x} \dot{x} + \frac{\partial A}{\partial y} \dot{y} + \frac{\partial A}{\partial z} \dot{z} \right\rangle = 0 \tag{10}$$

from which follows the relation between the moments

$$\langle x^k y^l z^m \rangle = \langle k, l, m \rangle \tag{11}$$

$$\begin{aligned} 0 = {} & k\sigma\langle k-1, l+1, m\rangle \\ & + l[(r-1)\langle k, l, m\rangle - (\sigma+1)\langle k, l, m\rangle \\ & - \langle k+1, l-1, m+1\rangle] \\ & + m[\langle k+1, l+1, m-1\rangle + \langle k+2, l, m-1\rangle - b\langle k, l, m\rangle] \end{aligned} \tag{12}$$

These relations could be helpful in constructing the probability distribution function. However, one must bear in mind that the number of moments grows faster with order $n = |k| + |l| + |m|$ than the number of relations connecting them. We list the first few relations, some of which will be used later:

$$\langle x^k y \rangle = 0, \qquad k = 0, \pm 1, \pm 2, \ldots \tag{13a}$$

$$\langle x^2 \rangle = b\langle z \rangle \tag{13b}$$

$$\langle xyz \rangle = -(\sigma+1)\langle y^2 \rangle \tag{13c}$$

$$\langle x(x+y)z \rangle = b\langle z^2 \rangle \tag{13d}$$

$$\langle x^2 z \rangle = \sigma\langle y^2 \rangle + (r-1)\langle x^2 \rangle \tag{13e}$$

$$b\langle x^2 z \rangle = 2\sigma\langle xyz \rangle + \langle x^4 \rangle \tag{13f}$$

The equalities (13b)–(13f) were reproduced numerically within a few parts per thousand for those r values plotted in Fig. 2. The above moments can

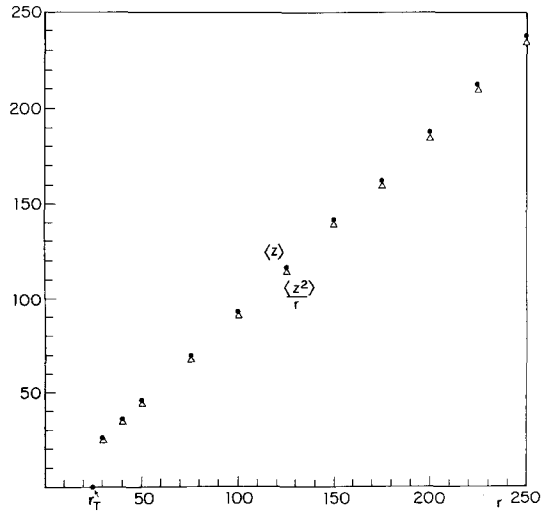

Fig. 2. Average values $\langle z \rangle$ (dots) and $\langle z^2 \rangle / r$ (triangles) for several values of r.

be expressed in terms of only two. For example, we can use $\langle z \rangle$ and $\langle z^2 \rangle$, which have the simplest behavior as a function of r.

Figure 2 shows the linear dependence of $\langle z \rangle$ on r, the slope being slightly less than one. $\langle z^2 \rangle$ contains r^2 terms, as can be seen from the plot of $\langle z^2 \rangle / r$ displayed also in Fig. 2. However, one should be careful in approximating $\langle z^2 \rangle$ by $\langle z \rangle r$, since then $\langle y^2 \rangle$, according to Eqs. (13c)–(13e),

$$\langle y^2 \rangle = b[(r - 1)\langle z \rangle - \langle z^2 \rangle] \tag{14}$$

would become negative. Numerically one finds $\langle y^2 \rangle$ to contain r^2 behavior.

Figure 2 indicates that the extrapolated value of $\langle z \rangle$ from above threshold $\langle z(r \to r_T) \rangle$ does not give the steady-state value $r_T - 1$. The associated discontinuous physical quantity is the heat flux, since in the Lorenz model z is proportional to the Nusselt number, which expresses the ratio of the total heat flux to the heat transported by conduction. A similar first-order phase transition at r_T was also found in a system of truncated Boussinesq equations consisting of 39 Fourier components.[13] These calculations[13] were done for Rayleigh–Bénard layers of low-Prandtl-number fluids, where the Lorenz model is no longer applicable. The experimental Nusselt number of helium, however, did not show a discontinuity at r_T.[14] The normalized fluctuations of z

$$\Delta_r(z) = \frac{\Delta(z)}{\langle z^2 \rangle^{1/2}} = \left(1 - \frac{\langle z \rangle^2}{\langle z^2 \rangle}\right)^{1/2} \tag{15}$$

are shown in Fig. 3 as a function of r. They increase upon approaching the threshold r_T from above.

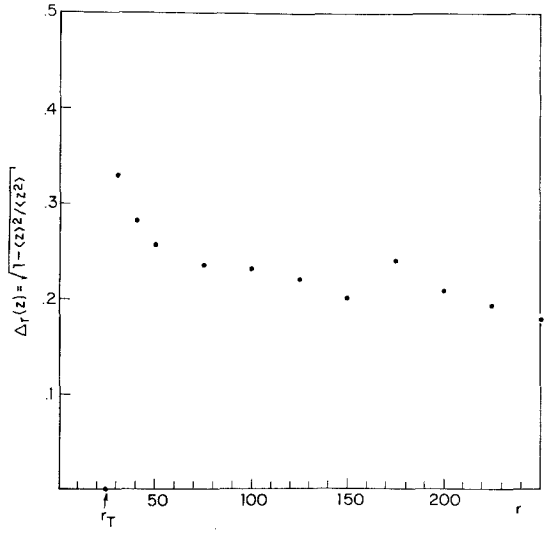

Fig. 3. Average normalized fluctuations $\Delta_r(z) = \Delta(z)/\langle z^2 \rangle^{1/2}$ [(15)] of z for various values of r.

3.3. Time-Dependent Correlations

The basic quantity to be calculated is the matrix of relaxation functions

$$\phi(t) = (S^0)^{-1} S(t) \tag{16}$$

with $S(t)$ the time-dependent matrix of correlations

$$S_{ij}(t) = \lim_{T \to \infty} \frac{1}{T} \int_0^T d\tau \, A_i(\tau) A_j(t + \tau) \tag{17a}$$

$$S_{ij}(t) = \langle A_i A_j(t) \rangle = S_{ji}(-t) \tag{17b}$$

between the variables

$$A_1 = x, \qquad A_2 = y, \qquad A_3 = \delta z = z - \langle z \rangle \tag{18}$$

S^0 denotes the diagonal matrix $S(t = 0)$ of initial values

$$S^0 = S(t = 0) = \begin{pmatrix} \langle x^2 \rangle & 0 & 0 \\ 0 & \langle y^2 \rangle & 0 \\ 0 & 0 & \langle (\delta z)^2 \rangle \end{pmatrix} \tag{19}$$

It is convenient to discuss the Laplace transform of $S_{ij}(t)$,

$$S_{ij}(z) = \left\langle A_i \frac{1}{z + L} A_j \right\rangle; \qquad \operatorname{Im} z > 0 \tag{20}$$

in terms of the time evolution operator L,

$$L = -i\partial_t \tag{21}$$

which allows us to formally write time-dependent functions $A(t)$ as

$$A(t) = e^{iLt} A \tag{22}$$

For later use we will introduce the scalar product between functions $A(t)$ and $B(t)$:

$$(A|B) = \langle A^* B \rangle = S^0_{AB} \tag{23}$$

With this scalar product the variables A_i of (18) are orthogonal.

Time translational invariance together with the fact that all occurring functions A and B will be real-valued implies that

$$(A|LB) = (LA|B) \tag{24}$$

i.e., $L = L^+$ is Hermitian and $S_{ij}(z)$ reads

$$S_{ij}(z) = \left(A_i \left| \frac{1}{z + L} \right| A_j \right) \tag{25}$$

$S_{ij}(z)$, being defined as a Laplace transform for $\mathrm{Im}\, z > 0$, has a spectral representation[9,15]

$$S_{ij}(z) = \int \frac{d\omega}{\pi} \frac{S''_{ij}(\omega)}{\omega - z} \tag{26}$$

for $\mathrm{Im}\, z \neq 0$. Since the discontinuity of $S_{ij}(z)$ along the real axis

$$S''_{ij}(\omega) = -\pi(A_i|\delta(\omega + L)|A_j) \tag{27a}$$

is here the imaginary part of S on the real axis, it is given[15] also by the Fourier transform $S_{ij}(t)$,

$$S''_{ij}(\omega) = -\tfrac{1}{2}\int_{-\infty}^{\infty} dt\, e^{i\omega t}\langle A_i A_j(t)\rangle \tag{27b}$$

Note that $-S''_{ii}(\omega)$ is real, positive, and even in ω.

Since LA_i has the same parity under the symmetry operation $x, y \to -x, -y$ as A_i, it follows that $S_{13} = S_{23} = S_{31} = S_{32} = 0$, so that

$$\phi(z) = \begin{pmatrix} \phi_{11}(z) & \phi_{12}(z) & 0 \\ \phi_{21}(z) & \phi_{22}(z) & 0 \\ 0 & 0 & \phi_{33}(z) \end{pmatrix} \tag{28}$$

The above form of the relaxation matrix is caused by parity and the linear decoupling of z from x and y in the differential equations (3).

Since these equations contain only two independent variables and a "conservation" law $\dot{x} = \sigma y$, only two independent relaxation functions, say $\phi_{22}(z)$ and $\phi_{33}(z)$, have to be calculated. Applying the equation of motion to the resolvent

$$z\frac{1}{z+L} = 1 - \frac{1}{z+L}L \tag{29}$$

one finds

$$z\phi_{12}(z) = -i(\Omega_0^2/\sigma)\phi_{22}(z) \tag{30}$$

$$z\phi_{21}(z) = i\sigma\phi_{22}(z) \tag{31}$$

$$z^2\phi_{11}(z) = z + \Omega_0^2\phi_{22}(z) \tag{32}$$

where the frequency Ω_0 is given by

$$\Omega_0^2 = \langle\dot{x}^2\rangle/\langle x^2\rangle \tag{33}$$

Figures 4 and 5 show the numerically obtained relaxation function $\phi_{22}(t)$ and $\phi_{33}(t)$ for three different values of r above threshold in the nonperiodic region. In both relaxation functions at least two different characteristic time

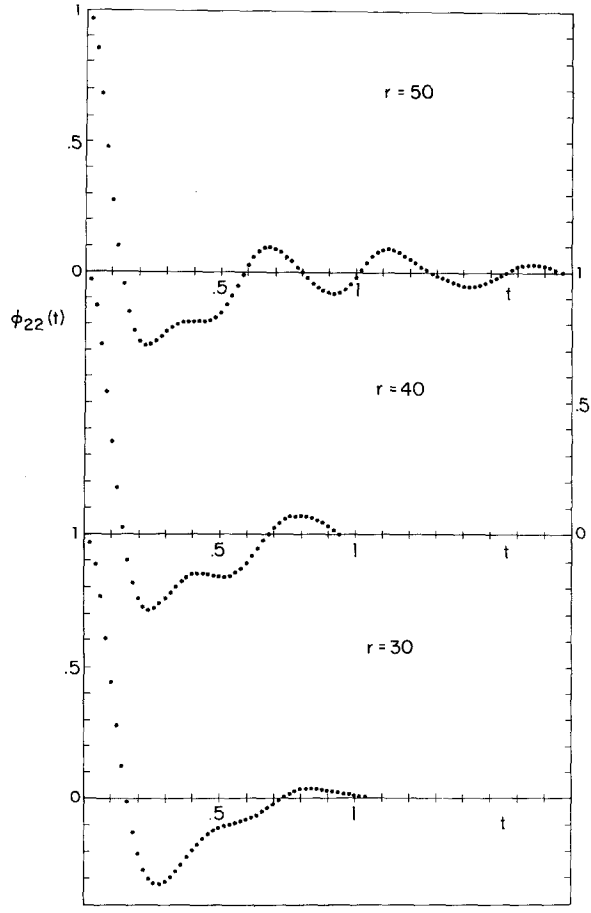

Fig. 4. Normalized relaxation function $\phi_{22}(t)$ for three values of r.

scales are present. Both correlations display a sharp initial decay of memory within a time of the order of 0.2, corresponding roughly to an average revolution of the phase point around one of the two steady-state points. This initial decay becomes more pronounced with increasing r. Then within a time of the order of 1, $\phi_{22}(t)$ phase mixes to zero, exhibiting a few irregular oscillations for the largest value of r. The time for complete loss of memory corresponds to the frequency of a complete revolution around both steady-state points.

$\phi_{33}(t)$ decays on a much longer time scale, exhibiting regular oscillations.[8] The frequency of these oscillations around the average value of z is roughly twice as big as that for a complete revolution of the trajectory around both steady-state points, which can be seen without calculation from

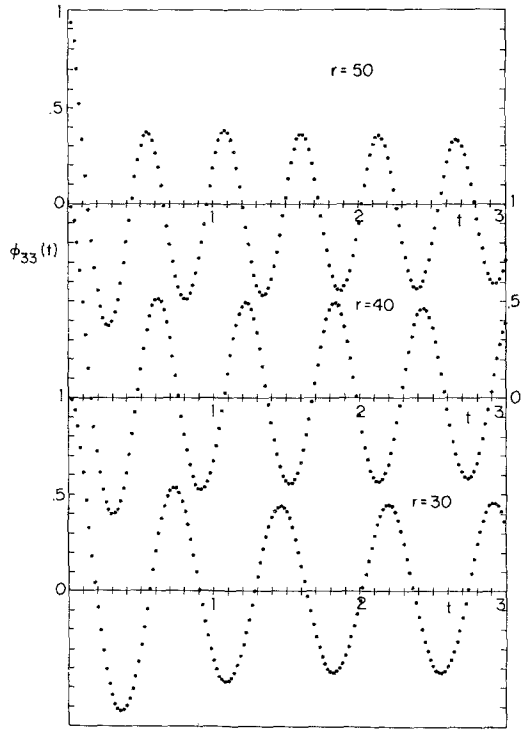

Fig. 5. Normalized relaxation function $\phi_{33}(t)$ for three values of r.

the form of the trajectories displayed in Fig. 1. These frequencies will be discussed in detail in the next section.

$\phi_{33}(t)$ is reproduced very well after one period by a simple, exponentially damped cosine oscillation with decay times of the order of 10 and oscillation frequencies ϵ which increase with increasing r. They will be discussed later.

3.4. Technical Details

All averages reported in this work were obtained on a Xerox Sigma 7 Computer using a four-point Runge Kutta procedure with time steps of 0.001 to integrate the system of differential equations (3) for several values of the parameter r with $\sigma = 10$ and $b = 8/3$ being fixed. For the r values discussed in this work an integration over a time interval $T = 150$ for equal time correlations and $T = 500$ for time-dependent correlations ensured numerical

convergence of the integrals of type (7) being evaluated as sums over rectangles.

An estimate for the errors due to the cutoff at $T = 500$ was obtained in a calculation of

$$\phi_{ii}(t; T) = \frac{1}{T}\int_0^T d\tau \, \frac{A_i(\tau)A_i(\tau + t)}{\langle A_i^2 \rangle} \tag{34}$$

done for $i = 2, 3$; $t = 0.1, 0.2, \ldots, 1.5$; $T = 500, 600, \ldots, 4900$ using time steps of 0.01. Since the variations of $\phi_{ii}(t; T)$ died out with increasing T, the maximal variation $\delta_{ii}(t)$ over the interval $T = 500$–4900 was used as an upper estimate for the cutoff errors: For values of t around the minima of $\phi_{33}(t)$ the cutoff error estimate $\delta_{33}(t)$ is three to four times the point size used in Fig. 5. Otherwise $\delta_{33}(t)$ as well as $\delta_{22}(t)$ are less than twice the point size used in Figs. 4 and 5, respectively, to plot the relaxation functions $\phi_{ii}(t)$.

An average of an expression A was set to zero when its reduced variance $\Delta_r(A) = (1 - \langle A \rangle^2/\langle A^2 \rangle)^{1/2}$ was unity within less than three parts per thousand. This is the reason for the cutoffs in Fig. 4. Figure 1 was plotted by a Hewlett Packard 9830 desk machine using the two-point procedure used by Lorenz[4] with a time increment of 0.01.

4. FLUCTUATION SPECTRA

4.1. Characteristic Frequencies

The motion of a phase space point as displayed in Fig. 1 is dominated by three different characteristic frequencies Ω_0, Ω_∞, and Ω_z. The low frequency Ω_0 of (33) accounts for complete revolutions around both steady-state points (5), whereas

$$\Omega_\infty{}^2 = \langle \dot{y}^2 \rangle / \langle y^2 \rangle = \langle \ddot{x}^2 \rangle / \langle \dot{x}^2 \rangle \tag{35}$$

characterizes high-frequency circular movements around one of the steady-state points (5). Finally,

$$\Omega_z{}^2 = \langle \dot{z}^2 \rangle / \langle (\delta z)^2 \rangle \tag{36}$$

measures the oscillation of $\delta z = z - \langle z \rangle$.

Note that the frequencies defined above are the simplest ones that can be formed from the variables A_i and $\dot{A}_i$ since

$$\langle \dot{A}_i / A_i \rangle = \langle A_i \dot{A}_i / A_i^2 \rangle = \tfrac{1}{2} \partial_t \langle \ln A_i^2 \rangle = 0 \tag{37}$$

Figure 6 shows the smooth increase of these frequencies proportional to $\sqrt{r}$.

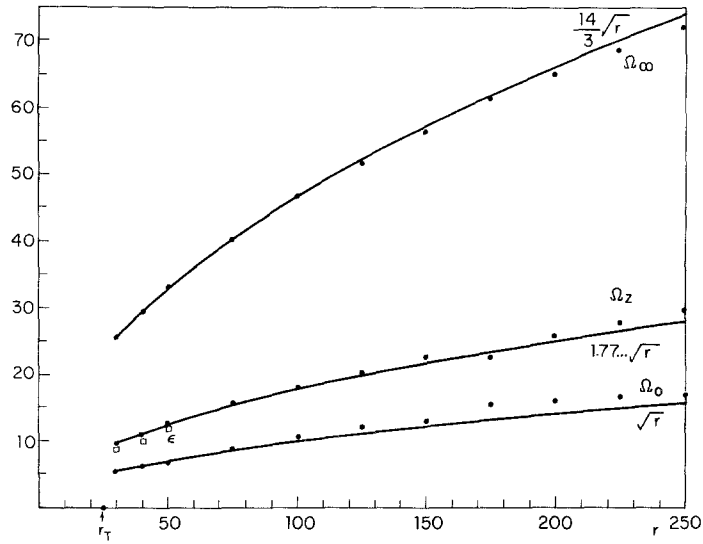

Fig. 6. Characteristic frequencies (dots) of the model for various values of r. Solid lines denote the curves $\sqrt{r}$, $1.77\ldots\sqrt{r}$, and $(14/3)\sqrt{r}$, respectively. Squares represent the oscillation frequencies ϵ of $\phi_{33}(t)$ according to Fig. 5.

Using the definitions (33), (35), and (36) and the moment relations (13), one finds

$$\Omega_0^2 = \sigma^2 \frac{\langle y^2 \rangle}{\langle x^2 \rangle} \tag{38a}$$

$$\Omega_\infty^2 = \frac{\langle x^2[z^2 - (r-1)^2] \rangle}{\langle y^2 \rangle} - 2\sigma(r-1) - (\sigma+1)^2 \tag{38b}$$

$$\Omega_z^2 = \frac{\langle y^2[x^2 + (\sigma+1)(2\sigma+b)] \rangle}{\langle z^2 \rangle - \langle z \rangle^2} \tag{38c}$$

These expressions, together with the fact that on the average $x^2 \sim z \sim r$ (Fig. 2) and $y^2 \sim r^2$ [(14)], explain the $\sqrt{r}$ behavior. The solid lines in Fig. 6 represent the graphs of $\sqrt{r}$, $1.77\ldots\sqrt{r}$, and $(14/3)\sqrt{r}$.

These relations imply that in the time $2\pi/\Omega_0$ during which the phase point moves from a minimal x value to a maximal one and back along the dumbbell-shaped trajectory displayed in Fig. 1 the y values either run through $14/3 \approx 5$ consecutive extrema along the same trajectory or circle around one of the steady-state points five times. The sign of δz, on the other hand, changes twice (1.78 times) as frequently as that of x.

The above prefactors can be written as $1.77\ldots = [(\sigma+1)/\sigma] + b - 2$ and $14/3 = \sigma - 2b$. Since these relations were not checked for different values of the parameters σ and b, they could be accidental.

Note that $\Omega_0(r \to r_T)$ does not tend to zero as a consequence of the behavior of $\langle y^2 \rangle$ [(14)] or $\langle z \rangle$ and $\langle z^2 \rangle$ displayed in Fig. 3. On the other hand, $\Omega_z(r \to r_T)$ seems to go toward the frequency ω_T,[6]

$$\omega_T = \left(2\sigma b \frac{\sigma + 1}{\sigma - b - 1}\right)^{1/2} \tag{39}$$

one finds studying the trajectories caused by linear perturbations from the steady-state solutions at the threshold $r = r_T$.

The squares in Fig. 6 represent the oscillation frequencies of $\phi_{33}(t)$ of Fig. 5, i.e., the peak positions ϵ in the spectrum of the A_3 motion. Thus, since Ω_z is only slightly bigger than ϵ, it is a characteristic frequency of the A_3 motion.

The relevance of the frequencies (38) for a theory of the relaxation spectra is manifested by restricting the shape of the spectra as sum rules according to (27a)

$$-\int_{-\infty}^{\infty} \frac{d\omega}{\pi} \omega^2 \phi_{ii}''(\omega) = \frac{(A_i|L^2|A_i)}{(A_i|A_i)} = \begin{cases} \Omega_0^2 & \text{for } i = 1 \\ \Omega_\infty^2 & \text{for } i = 2 \\ \Omega_z^2 & \text{for } i = 3 \end{cases} \tag{40}$$

The zeroth sum rule of the relaxation spectra reads

$$-\int \frac{d\omega}{\pi} \phi_{ii}''(\omega) = 1 \tag{41}$$

Incorporating characteristic frequencies or sum rules into a theory for relaxation spectra is not a new problem. The sum rules connected with density and current fluctuations in fluids, for example, are conveniently dealt with in continued fraction representations[15,16] of the Laplace-transformed correlation functions using relaxation kernels and dispersion relations.[9]

4.2. Relaxation Kernels and Dispersion Relations

Here the relaxation functions $\phi_{ij}(z)$ will be expressed by relaxation kernels and sum rules in a continued fraction representation. We therefore introduce the projector P[10] on the linear variables A_i,

$$P = |A_i)(S^{0-1})_{ij}(A_j| \tag{42}$$

and the orthogonal complement

$$Q = 1 - P \tag{43}$$

Both are Hermitian. Exploiting the resolvent identity

$$P\frac{1}{z+L}P\left[z+PLP-PLQ\frac{1}{z+QLQ}QLP\right]=P \tag{44}$$

and Eq. (25), one finds

$$\phi(z)=[z+\omega-M(z)]^{-1} \tag{45}$$

where the frequency matrix ω is given by

$$\omega_{ik}=(S^{0-1})_{ij}(A_j|L|A_k) \tag{46}$$

The relaxation kernels

$$M_{ik}(z)=(S^{0-1})_{ij}(A_j|LQ\frac{1}{z+QLQ}QL|A_k) \tag{47}$$

are correlation functions in whose time development linear variables are projected out.[15] The resolvent $[z+QLQ]^{-1}$ generates only nonlinear combinations in a function subspace orthogonal to the one containing linear combinations of A_i. A successive projection procedure can now be applied to $M(z)$ which yields a result similar to (45), thus generating a further step in the continued fraction. Each successive kernel $M(z)$ has the same analytic properties and symmetries[15] as the original relaxation function $\phi(z)$. In particular $M(z)$ can be given a spectral representation like Eq. (26) which connects its real part $M'(\omega)$ and imaginary part $M''(\omega)$ along the real axis by a Kramers–Kronig dispersion relation

$$M'(\omega)=P\int\frac{d\omega'}{\pi}\frac{M''(\omega')}{\omega'-\omega} \tag{48}$$

Exploiting parity and time translational invariance, one finds for the frequency matrix (46)

$$\omega=i\Omega_0\begin{pmatrix}0 & \Omega_0/\sigma & 0\\ -\sigma/\Omega_0 & 0 & 0\\ 0 & 0 & 0\end{pmatrix} \tag{49}$$

The matrix of memory kernels (47) has the form

$$M(z)=\begin{pmatrix}0 & 0 & 0\\ 0 & M_{22}(z) & 0\\ 0 & 0 & M_{33}(z)\end{pmatrix} \tag{50}$$

Inserting (49) and (50) into (45), one finds $\phi(z)$ to be of the form (28) as well

as the equation of motion relations (30)–(32). The two independent relaxation functions read

$$\phi_{22}(z) = z \frac{1}{z^2 - \Omega_0{}^2 - zM_{22}(z)} \tag{51}$$

$$\phi_{33}(z) = \frac{1}{z - M_{33}(z)} \tag{52}$$

The memory kernels $M_{22}(z)$ and $M_{33}(z)$ reflect the nonlinear coupling of the x, y motion in Eq. (3).

Let us discuss $M_{33}(z)$ first. From Fig. 5 one infers that $\phi_{33}(z)$ must have poles at frequencies $z = \pm\epsilon - i/\tau$, $1/\tau$ being small compared to $\epsilon \sim \Omega_z$ as plotted in Fig. 6. Such a pole structure is easily generated by representing $M_{33}(z)$ by a kernel $\gamma_{33}(z)$. Repeating the projection procedure (44), one finds

$$\phi_{33}(z) = \frac{z - \gamma_{33}(z)}{z^2 - \Omega_z{}^2 - z\gamma_{33}(z)} \tag{53}$$

with $\gamma_{33}(z)$ given by

$$\gamma_{33}(z) = \frac{1}{\Omega_z{}^2} (A_3|(L^2 - \Omega_z{}^2) \frac{1}{z + \tilde{Q}QLQ\tilde{Q}} (L^2 - \Omega_z{}^2)|A_3) \frac{1}{(A_3|A_3)} \tag{54}$$

The projector $\tilde{P} = 1 - \tilde{Q}$ projects onto $QL|A_3)$, being orthogonal to the original variables A_i.

The approximation

$$\gamma_{33}(z) = 0 \tag{55a}$$

or

$$(L^2 - \Omega_z{}^2)|A_3) = 0 \tag{55b}$$

would describe an undamped periodic motion of the A_3 component with frequency Ω_z. Actually, the frequency ϵ of the A_3 movement is a little smaller than Ω_z (cf. Fig. 6) and is slightly damped. That means that a single time relaxation approximation is reasonable,

$$\gamma'_{33}(\omega) = 0; \qquad \gamma''_{33}(\omega) = -\gamma \tag{56a}$$

$$\phi''_{33}(\omega) = -\gamma\Omega_z{}^2/[(\omega^2 - \Omega_z{}^2)^2 + \omega^2\gamma^2] \tag{56b}$$

This yields for $\gamma \ll \Omega_z$ a sharp peak shifted to a smaller frequency than Ω_z as required by Fig. 5.

4.3. Mode Coupling

In the following section it will be demonstrated that a simple mode coupling picture for M_{22} consistently explains the spectrum $\phi''_{22}(\omega)$ of the A_2

motion. As discussed following Fig. 4, it is not dominated by a single frequency and will thus be more complicated than that of the A_3 motion. It exhibits, according to Eq. (51), an oscillator spectrum determined by the static restoring frequency Ω_0—note that (32) implies $(1/z)\phi_{22}(z)|_{z=0} = -\Omega_0^{-2}$—and the complex damping kernel $M_{22}(z)$

$$M_{22}(z) = (A_1A_3|Q\frac{1}{z+QLQ}Q|A_1A_3)\frac{1}{S_{22}^0} \tag{57}$$

which represents the coupling of the A_1 or A_2 variable to all other nonlinear combinations of the A_i. The spectrum of the kernel is dominated by spectra of the coupled A_1A_3 motion, as indicated by the form (57) representing correlations of the nonlinear variables A_1A_3.

Within mode coupling procedures the spectrum $M_{22}''(\omega)$ is approximated by a convolution of the spectra of the two "modes" corresponding to the A_1 and A_3 motion. Thus

$$M_{22}''(\omega) \sim \phi_{11}''(\omega) * \phi_{33}''(\omega) \tag{58}$$

Since the relaxation spectrum $\phi_{33}''(\omega)$ can well be approximated by δ functions at frequencies $\pm\epsilon$, one finds

$$M_{22}''(\omega) \sim [\phi_{11}''(\omega-\epsilon) + \phi_{11}''(\omega+\epsilon)] \tag{59}$$

The spectrum

$$\phi_{11}''(\omega) = (\Omega_0^2/\omega^2)\phi_{22}''(\omega) \tag{60}$$

turns out to be a more or less smooth Lorentzian-shaped curve with half-width $\Gamma \simeq 1.2\Omega_0$. As explained following Fig. 4, the correlations of A decay within a time of the order of $1/\Omega_0$, which gives rise to the above described Lorentzian: For our purposes it is sufficient to use in the relaxation kernel a Lorentzian for $\phi_{11}''(\omega)$, which gives

$$M_{22}(z) = \frac{\Delta^2}{2}\left(\frac{1}{z-\epsilon+i\Gamma} + \frac{1}{z+\epsilon+i\Gamma}\right) \tag{61}$$

and

$$\phi_{22}(z) = z\left[z^2 - \Omega_0^2 - z\frac{\Delta^2}{2}\left(\frac{1}{z-\epsilon+i\Gamma} + \frac{1}{z+\epsilon+i\Gamma}\right)\right]^{-1} \tag{62}$$

The value of Δ measuring the strength of the "vertex" for the interaction of A_1 and A_3 modes has still to be determined. There are several possibilities.

One is to ensure the correct high-frequency behavior of $\phi_{22}(z)$ by adjusting Δ^2 to the first sum rule of $M_{22}(z)$. That would require

$$\Delta^2 = \frac{(\dot{y}|LQL|\dot{y})}{(\dot{y}|\dot{y})} = \frac{\langle\ddot{y}^2\rangle}{\langle\dot{y}^2\rangle} - \frac{\langle\dot{x}^2\rangle}{\langle x^2\rangle} \tag{63a}$$

$$= \Omega_\infty^2 - \Omega_0^2 \tag{63b}$$

which gives, according to Fig. 6, values of Δ roughly 4–5 times larger than Ω_0. However, such a high frequency does not play an important role in the spectra which are centered around Ω_0 and Ω_z.

So the other possibility for determining Δ by enforcing the correct low-frequency behavior is more promising. From (32) and (51), we find the exact relation

$$\phi''_{11}(\omega = 0) = M''_{22}(\omega = 0)/\Omega_0{}^2 \tag{64}$$

which is the generalized version of a Kubo formula.[9,15] Note that all relaxation functions $\phi''_{ii}(\omega)$ as well as the kernels $M''_{ii}(\omega)$ are even in ω, causing the odd, real parts to vanish at $\omega = 0$. If $\phi''_{11}(\omega)$ were really a Lorentzian, (64) together with (61) would uniquely determine Δ^2 to be

$$\Delta^2 = \Omega_0{}^2[1 + (\epsilon^2/\Gamma^2)] \tag{65}$$

thus imposing a self-consistency condition upon the spectrum $\phi''_{11}(\omega)$.

Figure 7 shows a comparison of the spectra $\phi''_{22}(\omega)$ (dots) obtained by Fourier-transforming the "experimental" data displayed in Fig. 4 with the theoretical results

$$\phi''_{22}(\omega) = \omega^2 \frac{M''_{22}(\omega)}{[\omega^2 - \Omega_0{}^2 - \omega M''_{22}(\omega)] + [\omega M''_{22}(\omega)]^2} \tag{66}$$

using the mode coupling approach (61) for the kernel $M_{22}(z)$. The parameters $\Gamma = 1.2\Omega_0$ and ϵ as shown in Fig. 6 are fixed by the experimental spectra $\phi''_{11}(\omega)$ and $\phi''_{33}(\omega)$ entering the mode coupling expression (58). The coupling strength Δ is determined by the self-consistency restriction (65).

The spectra displayed in Fig. 7 are rather broad. On the low-frequency side they show an ω^2 increase, reflecting the "conservation" law (32). There is a long, high-frequency tail extending to values as high as Ω_∞. The main peak of the spectrum according to experiments is slightly above Ω_0, whereas the theoretical peak position is roughly located at Ω_0.

The spectra show a secondary peak or shoulder well above Ω_0 which cannot be explained in terms of the characteristic frequencies Ω_0 and Ω_∞. According to Eqs. (51) and (57), this high-frequency structure is caused by the coupling of A_2 motion to the A_3 motion represented by a coupling function $M''_{22}(\omega)$ of the form (58). The presence of such a coupling term causes the relaxation function $\phi_{22}(z)$ [(62)] to have a pole whose position in the lower half of the complex plane is pushed out toward frequencies greater than Ω_0 with increasing coupling strength Δ.

The broad type of the spectra is explained by the fact that neither of the extreme cases, Δ much smaller or much larger than Ω_0 or Γ, is realized according to Eq. (65). The theoretical spectra are skewed toward lower

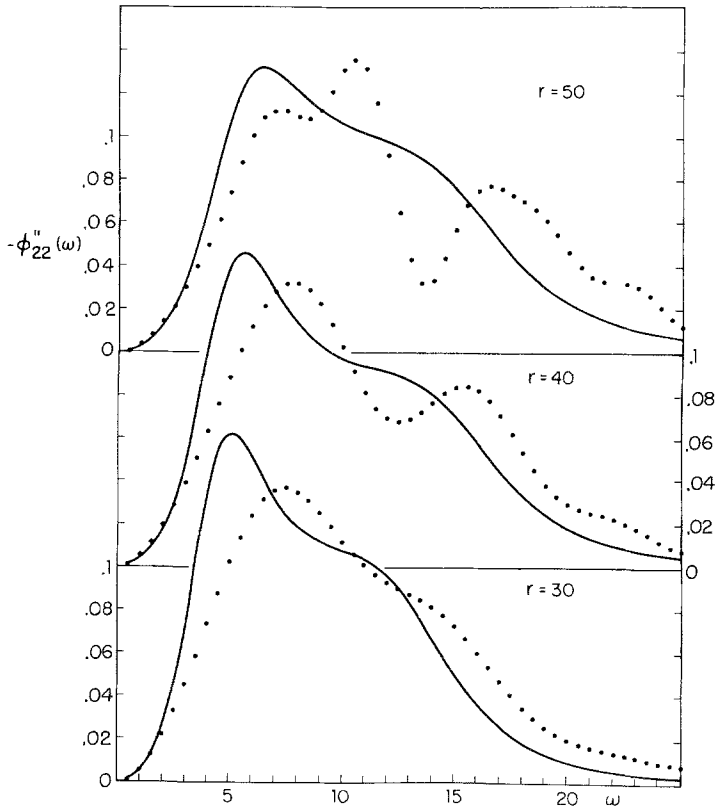

Fig. 7. Spectrum $-\phi''_{22}(\omega)$ (dots) compared with the theoretical result (66) for three values of r.

frequencies compared to "experiments," indicating too small a coupling strength Δ. Increasing Δ shifts the whole spectrum toward higher frequencies.

Note that Δ was determined by the zero-frequency value $\phi''_{11}(0)$ assuming $\phi''_{11}(\omega)$ to be a Lorentzian. With increasing r the experimental spectra display more structure, indicating that, according to Lorenz,[5] the system approaches a periodic regime with increasing r. Thus one is no longer justified to approximate $\phi''_{11}(\omega)$ in the relaxation kernel (59) by a smooth Lorentzian, which, because of (66), causes the theoretical spectra to be too smooth. To solve such a problem self-consistently is feasible[17] but requires more numerical effort.

Since the objective of this paper was to explain the statistical dynamics of the model, we neither tried to minimize nor optimize the choice of parameters. Even so this simple mode coupling approximation reproduces with only two fixed parameters $\epsilon/\Omega_0 \approx \Omega_2/\Omega_0 \approx 1.78$ and $\Gamma/\Omega_0 \approx 1.2$ and the

characteristic frequency $\Omega_0 \approx \sqrt{r}$ the spectra $\phi''_{22}(\omega)$ reasonably well for r values not too far above threshold.

5. SUMMARY

The basic goal of this paper was to show that the dynamics of the Lorenz model above the "turbulence" threshold could be described by using standard methods for the statistical treatment of many-body systems.

Time translational invariance of averages and the inversion symmetry of the model-defining equations were used to derive relations between various correlations functions and to reduce the nine relaxation functions of the model to only two independent ones.

The three simplest averaged frequencies to be defined by the variables of the model were shown to characterize its phase space motion. These characteristic frequencies increase in proportion to $\sqrt{r}$.

The spectra of the two independent relaxation functions evaluated numerically for three different values of r were explained in a standard dispersion relation representation for correlation functions generated by a Mori–Zwanzig projector formalism. From this scheme emerged continued fraction expressions involving the characteristic frequencies and two different relaxation kernels.

It was demonstrated why one of the kernels is very small, thus causing the δ-function-like spectrum of the z motion and the shifting of the peak position to a slightly lower frequency than the corresponding characteristic frequency.

The other spectrum is much broader, exhibiting structure which was shown to be a consequence of the nonlinear coupling of the motion of the three variables. This nonlinear coupling of the modes is expressed by the relaxation kernel. A simple mode coupling approximation for the spectrum of the kernel, with the coupling strength of the modes determined by a self-consistency condition imposed on the spectra involved, reproduced semi-quantitatively and explained the second "experimental" spectrum for several values of r.

ACKNOWLEDGMENTS

I wish to thank P. C. Martin for several helpful discussions and for his hospitality. Discussions with E. N. Lorenz, J. B. McLaughlin, and D. R. Nelson as well as C. D. Gelatt's advice in computational problems are gratefully acknowledged. This work was supported in part by National Science Foundation Grant No. DMR 72-02977 A03.

REFERENCES

1. P. C. Martin, talk given at International Conference on Statistical Physics, Budapest, 1975, to be published.
2. R. M. May, *Science* **186**:645 (1974); R. M. May and G. F. Oster, *Am. Natur.* **110**:573 (1976).
3. G. F. Oster, to be published.
4. E. N. Lorenz, *J. Atmos. Sci.* **20**:130 (1963).
5. E. N. Lorenz, to be published.
6. J. B. McLaughlin and P. C. Martin, *Phys. Rev. A* **12**:186 (1975).
7. S. A. Orszag, *Proceedings of the 1973 Les Houches Summer School of Theoretical Physics*, to be published.
8. J. B. McLaughlin, Ph.D. thesis, Harvard University (1974), unpublished; and private communication.
9. L. P. Kadanoff and P. C. Martin, *Ann. Phys. (N.Y.)* **24**:419 (1963); P. C. Martin, in *Problème à N corps*, C. de Witt and R. Balian, eds. (Gordon and Breach, New York, 1968).
10. R. Zwanzig, in *Lectures in Theoretical Physics*, W. Brittin and L. Dunham, eds. (Wiley–Interscience, New York, 1961), Vol. 3, p. 135; H. Mori, *Prog. Theor. Phys.* **33**:423 (1965); **34**:399 (1965).
11. B. Salzman, *J. Atmos. Sci.* **19**:329 (1962).
12. D. Ruelle and F. Takens, *Comm. Math. Phys.* **20**:167 (1971).
13. J. B. McLaughlin and P. C. Martin, *Phys. Rev. Lett.* **33**:1189 (1974).
14. G. Ahlers, *Phys. Rev. Lett.* **33**:1185 (1974).
15. D. Forster, *Hydrodynamic Fluctuations, Broken Symmetry, and Correlation Functions* (W. A. Benjamin, Reading, 1975).
16. J. R. D. Copley and S. W. Lovesey, *Rep. Prog. Phys.* **38**:461 (1975).
17. W. Götze and M. Lücke, *Phys. Rev. A* **11**:2173 (1975); *Phys. Rev. B* **13**:3825 (1976).